Wetting of a dynamically patterned surface is a time-dependent matter

Wanlin Chen,[†,‡] Ondřej Kroutil,[¶] Milan Předota,[¶] Simone Pezzotti,[*,§] and Marie-Pierre Gaigeot[*,†,‖]

†*Université Paris-Saclay, Univ Evry, CY Cergy Paris Université, CNRS, LAMBE UMR8587, 91025 Evry-Courcouronnes, France*

‡*Current Address: Department of Physical Chemistry II, Ruhr University Bochum, D-44801 Bochum, Germany*

¶*Department of Physics, Faculty of Science, University of South Bohemia, Branišovská 1760, 370 06 České Budějovice, Czech Republic*

§*PASTEUR, Département de Chimie, Ecole Normale Supérieure, PSL University, Sorbonne University, CNRS, 75005 Paris, France*

‖*Institut Universitaire de France (IUF), 75005 Paris, France*

E-mail: simone.pezzotti@ens.psl.eu; mgaigeot@univ-evry.fr

Abstract

In nature and many technological applications, aqueous solutions are in contact with patterned surfaces, which are dynamic over timescales spanning from ps to μs. In biology, exposed polar and apolar residues of biomolecules form a pattern, which fluctuates in time due to sidechain and conformational motions. At metal/ and oxide/water interfaces the pattern is formed by surface topmost atoms, and fluctuations are due to, e.g., local surface polarization and rearrangements in the adsorbed water layer. All these dynamics have the potential to influence key processes such as wetting, energy

relaxation, and biological function. Yet, their impact on the water H-bond network remains elusive. Here, we leverage on molecular dynamics to address this fundamental question at a Self-Assambled Monolayer (SAM)/water interface, where ns dynamics is induced by frustrating SAM-water interactions via methylation of the terminal -OH groups. We find that surface dynamics couples to the water H-bond network, inducing a response on the same ns timescale. This leads to time fluctuations of local wetting, oscillating from hydrophobic to hydrophilic environments. Our results suggest that more than average properties, it is the local—both in time and space—solvation that determines the chemical-physical properties of dynamically patterned surfaces in water.

Introduction

The way surfaces are wetted by aqueous solutions determines their chemical and physical properties in a vast range of natural phenomena and industrial applications.[1–11] The surface topology, i.e. the patterns formed by polar and apolar groups over the surface, and the morphology, e.g., concave *vs* convex geometry, have been recognized as key parameters dictating wetting and the many related chemical-physical properties.[1,3,12–26] The molecular understanding of these complexities is an emerging research area, whose relevance span across many fields. For instance, the pattern formed by the residues in a protein dictates its local hydrophilicity/phobicity, which in turn determines its capability to bind substrates, its folding/unfolding, its phase separation behavior, to cite a few.[1,2,15–18,27–34] As summarized in a recent review from Rego and coworkers,[1] more than the total fraction of polar and apolar residues exposed to water, it is the way they are distributed over the surface and the local surface morphology that matters. This is because hydrophobicity depends not on single water-surface interactions, but on the collective rearrangement of the water H-bond network in response to the distribution of polar groups at the surface.[17] At oxide/water interfaces - of relevance in, e.g., geochemistry and heterogeneous catalysis - the pattern formed by the oxide surface OH terminations influences the interfacial free energy, the vibrational

and optical properties, ions adsorption (hence the structure of the electric double layer) and even the chemistry.[3,20–22,35–38] A prominent example are amorphous silica surfaces, where polar (SiOH) and apolar (SiOSi) terminations are inhomogeneously distributed, giving rise to hydrophilic (SiOH rich) and hydrophobic (SiOSi rich) patches with distinct water H-bond network arrangments, whose size can be tuned by changing the way the surface is pre-treated.[20,36,37,39–41] In electrochemistry, hydrophobicity arises due to the strongly adsorbed water adlayer formed in contact with metal surfaces (as well as with some oxides), which induces the formation of a water-water interface with low H-bond connectivity close to the electrode.[19,42–46] Exploiting such hydrophobicity is more and more regarded as a promising avenue for regulating adsorption and electrocatalysis.[45,47–53] There, once more, hydrophobicity is a local property, which can vary dynamically on a nano-meter size-scale, depending on local electrode surface polarization, adsorption/functionalization, and slow rearrangements in the adsorbed water layer.[19,50,52,54]

Strikingly, in most cases, surface properties are not static, but change dynamically, with timescales spanning from 10' ps to μs. For example for biomolecules, sidechain dynamics occur on the 1-10 ns timescale, and conformational dynamics occur on up to μs timescales, both possibly altering the biomolecules' patterns exposed to water.[55–57] For electrified metal/water interfaces, the fluctuations of the water adlayer can take place on distinct time-scales, from 10' ps to ns, and alter the local wetting, depending on the strength of metal-water interactions and surface pattern.[19,43,54] All these dynamics have the potential to modulate the response of water close to the surface, therefore wetting in a time-dependent way, inducing water network fluctuations that may have crucial implications for biological and electrochemical processes.[1,11,19,54,58,59] While we are continuously advancing our molecular understanding on the connections between wetting and surface patterns, as well as on the implications for interfacial chemistry, we have been mostly limited to investigate average properties. The effect of surface dynamics on the repsonse of water to patterned surfaces remains much less explored, despite the coupling between water and surface modes is well recognized to play

a crucial role for energy relaxation, interfacial (ultra-fast) dynamics, electrochemical properties, as well as biological function in the case of proteins.[21,58–64] The present work focuses on this gap of knowledge.

We explore the effect of the dynamics of a patterned surface on its wetting properties at the molecular level by means of ab-initio (DFT-based) and classical molecular dynamics (DFT-MD and CMD) simulations. We consider Self-Assembled Monolayer (SAM)/water interfaces that were previously characterized in detail from DFT-MD and Sum Frequency Generation (SFG) spectroscopy.[65,66] In order to induce dynamics in the surface patterns, the SAM is composed of methylated-PEG (mPEG) units, which terminate with a -O-CH_3 group instead of -OH. The terminal methylation of PEG chains frustrates SAM-water interactions: the -CH_3 groups are apolar and interact much more weakly with water than the adjacent O atoms. Either of them can be exposed to water depending on the PEG chain conformation: even a small change in the terminal torsional angle of the PEG chains is sufficient to locally switch from a hydrophilic patch, rich in exposed -O- atoms to a more hydrophobic patch, rich in exposed -CH_3 groups. This creates a dynamicity in the local pattern of the SAM surface exposed to water that evolves on a ns time scale. By analyzing the water H-bond network response from the simulations, we show hereby that water is sensitive to the local variations in the surface patterns and fastly reacts to these perturbations by rearranging its H-bond network, with a strong influence on local wetting.

Methods

We combine DFT-MD (previously performed in ref. 66, at the BLYP-D2 level[67–70]) and CMD simulations of mPEG-SAM/water interfaces (with mPEG anchored on a silica substrate). The DFT-MD simulations with the chosen set-up were previously found to provide a good description of the interface and its wetting properties, as validated against SFG experiments and contact angle measurements.[66] These simulations are here used as a reference to assess

the quality of CMD in describing the interfacial molecular arrangement (in terms of both H-bond network arrangement and SFG spectroscopy, see Fig. 1), as well as to get information on interfacial structure and dynamics at small length-scale, with box dimensions of 13×13×85 Å^3, and short time scales ($\sim$ 100 ps). The CMD simulations are used to quantify the ns dynamics of the surface patterns and of the water H-bond network response on a larger scale. All CMD simulations are performed with the GROMACS package.[71]

The choices of force fields for the different parts of the system are based on the setup of ref. 72. The CLAY force field,[73] which was shown to reproduce sufficiently well the structure of quartz/water interfaces,[74] is adopted for the silica substrate on which the SAMs are anchored. SAM polymers are described using the same set-up as in ref. 72, consisting of the AMBER force field,[75] coupled with the RESP method[76] for the partial charges determination. We use the SPC-Marti model[77] for water, which is a flexible SPC-based model, shown to describe sufficiently well the molecular vibrations[78] thanks to the implementation of bond-bond, bond-angle, and angle-angle cross terms in the intramolecular part of the force field. The Lorentz-Berthelot combining rules are adopted for interactions between nonbonded atoms.

Four independent CMD simulations of mPEG/water were performed. For all of them, an equilibration run of 10 ns in the NVT ensemble has been carried out, followed by an NVT production run (1 ns or 80 ns, see table 1 for details), using a Nose-Hoover thermostat[79,80] and with a time-step of 0.1 fs. The coordinates and velocities are saved at different frequencies depending on the length of the production runs (see table 1 for details). Two box sizes were chosen in the CMD simulations: 13×13×85 Å^3 (same as the DFT-MD system, denoted 1×1 in the following) and 40×40×300 Å^3 (9 times the DFT-MD size, denoted 3×3). 3D periodic boundary conditions have been applied.

We evaluate hydrophilicity/phobicity of the interface from these simulations, and connect it to the H-bond properties within the topmost interfacial layer (usually named Binding Interfacial Layer, BIL),[20,21,66,82,84–87] by means of a recently introduced x_H descriptor.[66] In short, we calculate the number of "horizontal" H-bonds (n_H) formed between water molecules

Table 1: List of CMD simulations for SAM (mPEG)/water interfaces

No.	Size (Å^3)	Length (ns)	Saved each (ps)	Ensemble
1	13×13×85	1	1	NVT
2	13×13×85	80	50	NVT
3	40×40×300	1	1	NVT
4	40×40×300	80	50	NVT

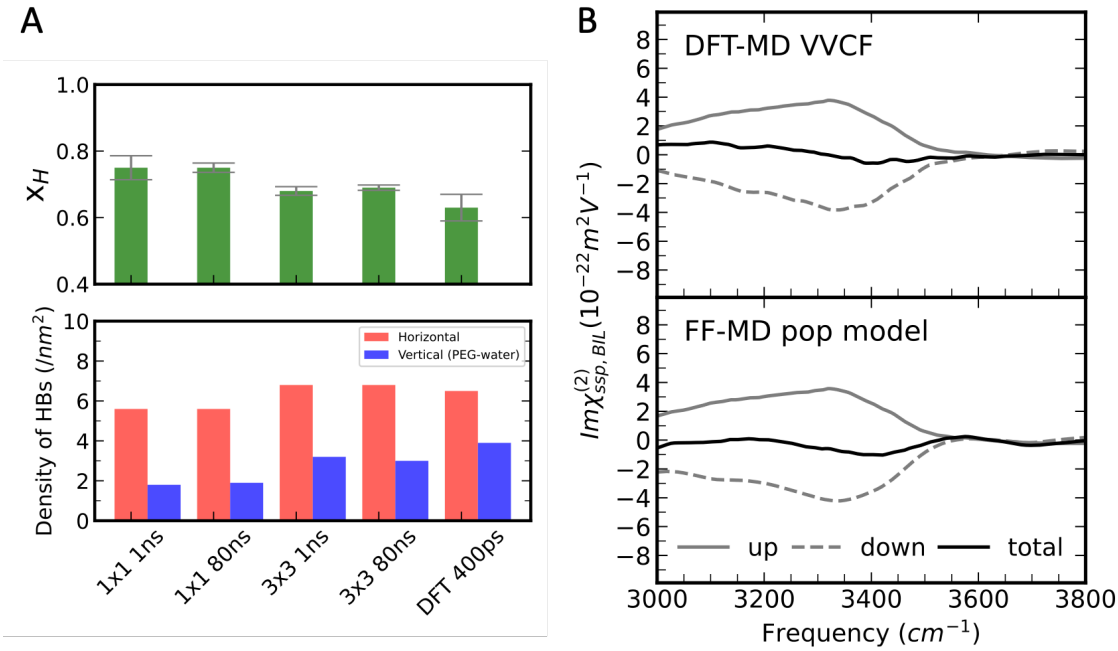

Figure 1: Validation of CMD simulations of mPEG/water against DFT-MD. (A) Averaged H/V values (x_H) obtained from CMD simulations of different time- and length-scales (error bars in grey) compared to the reference DFT-MD simulation (400 ps). Bottom: densities of "Horizontal" and "Vertical" H-bonds formed by BIL-water, as defined in the text, from which x_H is computed according to eq. 1. A good agreement is found between the reference DFT-MD and the CMD simulations on a large 3×3 box. (B) BIL-water SFG spectrum of the mPEG/water interface from DFT-MD (upper panel, using the VVCF method[81,82]) *vs* the CMD simulation of 80 ns on the 3×3 box (lower panel, using the "pop model" approach of ref. 83). The total BIL-SFG spectrum is shown together with the deconvolved contributions from BIL-water OH groups pointing toward the SAM (up, solid grey) and toward the liquid phase (down, dashed grey). Both the total spectra and the deconvolved up and down components show a very good agreement.

in the BIL, which are by construction oriented parallel to the instantaneous water surface[88] in contact with SAMs ± 30°(since the BIL at these interfaces consists of 1 water monolayer, see all details in ref. 66. We then define the mole fraction x_H of horizontal H-bonds as our

H/V descriptor:

$$H/V = x_H = \frac{n_H}{n_H + n_V} \tag{1}$$

where n_V refers to "vertical" H-bonds formed between water and surface atoms (mPEG -O- atoms in the present system). Horizontal and vertical H-bonds are not defined based on orientation, rather based on H-bond partners: horizontal for BIL-water–BIL-water H-bonds, vertical for BIL-water–surface H-bonds. The H/V descriptor evaluates wetting based on the competition between the horizontal and vertical components of the H-bond networks. The concept is that the water H-bond network arranges close to hydrophobic surfaces, such as at the air/water interface, by maximizing the "horizontal" H-bonds formed between BIL-water molecules and forming extended 2D-H-bond-network (2DN) structures.[40,89,90] This is needed to compensate for the lack of ("vertical") water-surface interactions and minimize the density of dangling OH groups, resulting in a preferential "horizontal" component in the interfacial H-bond network.[40,89,90] Instead, strong surface-water interactions, of same or higher strength that water-water H-bonds, can locally rearrange the water network from the 2DN structure that uniformly covers a purely hydrophobic surface, with a local increase in "vertical" water-surface H-bonds and a consequent decrease in "horizontal" H-bonds. This is also the reason why weak interactions between water and CH_3 groups of PEG are not considered for the H/V analysis: these interactions are weaker then water-water and water-O(PEG) H-bonds (as confirmed by both structural anbd spectroscopic analysis),[66] and therefore do not dictate the balance between the two H-bonds motifs, despite contributing to the total interfacial free energy.

BIL-water maximizes vertical interactions with the surface in contact with hydrophilic surfaces.[66,86,90] Therefore, the lower the x_H is, the more hydrophilic the interface is. To put this descriptor into context, useful reference values are $x_H = 1.0$ for the prototypical hydrophobic air/water interface, and $x_H = 0.5$ for a typical hydrophilic interface like α-Quartz/water (sometimes referred to as superhydrophilic). x_H was shown to quantitatively describe hydrophilicity, since it well correlates with contact angle measurements, as well as

with spectroscopic evaluations of hydrophobicity (by the amplitude of the free-OH band), for several SAM/water interfaces of varying hydrophilicity, including the mPEG/water discussed here.[66] The advantage, for the purpose of the present study, is that x_H is defined based on local H-bond properties, hence allowing a local description of hydrophilicity with spatial and temporal resolutions.

A similar H-bond based descriptor has been also tested against most common local hydrophobicity descriptors based on water density fluctuations,,[1,16–18,24,35,43,91–93] on a few solvated proteins,[28] providing a similar identification of hydrophobic and hydrophilic patches. A correlation between the hydrophobicity measured by means of water density fluctuations and the H-bonding network properties in the BIL was recently highlighted also for oxide/water interfaces.[35] This provides a further validation of the x_H descriptor. Compared to density fluctuation-based approaches, which have been recently successfully exploited in advanced computational methods to map local hydrophobicity of biomolecules,[18] x_H has a less direct connection to thermodynamics (at the advantage of a more direct connection to spectroscopic quantities),[66] as well as a less direct connection to basic concepts of hydrophobic solvation theories.[2,94] However, its application to time-resolved analysis is more straightforward and does not require coupling to enhanced sampling methods, making it a very suitable choice for the present study.

Fig. 1A reports a comparison between x_H values from DFT-MD and CMD simulations of the mPEG/water interface. All simulations provide average x_H values in the 0.65–0.75 range, closer to the value of 0.5 of α-Quartz/water than that of 1.0 of air/water, hence indicating a (moderately) hydrophilic surface. The CMD simulations with the 1x1 box overestimate the x_H compared to that of DFT-MD, while the big 3x3 box describes well the x_H property. Based on this, all CMD results discussed hereafter have been calculated on the 3x3 simulations. To further validate the CMD simulations, the theoretical SFG spectrum is also calculated from the simulation of a 3x3 box by using the pop model approach developed in ref. 83, which shows very good agreement with DFT-MD calculated spectrum from ref.

66, see Fig. 1B. Since SFG spectroscopy in the OH-stretching range is extremely sensitive to the H-bond connectivity and orientation of interfacial water, such a good agreement is an important proof that CMD and DFT-MD descriptions of the mPEG/water interface are coherent with each other.

For all analyses, two different distance+angle H-bond criteria have been systematically compared, with O–O distances of 3.2 and 3.5 Å, and O–H–O angles of 0±40 and 0±30 degrees, respectively,[95,96] providing the same results in terms of x_H values. BIL-water molecules are defined at each MD step as all water molecules whose O-centers are located <3.4 Å from the instantaneus Willard-Chandler surface,[88] according to the results of ref. 66.

Results and discussion

Surface pattern dynamics at the mPEG/water interface

To understand the surface patterns of mPEG in contact with water, we calculate the density maps of mPEG atoms (both carbon and oxygen) exposed to water, projected on the surface xy-plane. C and O atoms of mPEG are considered exposed to water if they are located within 3 Å below the Willard and Chandler (WC) instantaneous water surface;[88] and their coordinates are projected onto the xy-plane to obtain the xy-maps. The time-resolved maps are calculated at different time periods along the trajectory to track the time evolution of the mPEG surface organization. Fig. 2A-F display representative density maps at three different time periods chosen from the DFT-MD simulation of 400 ps, A-C for carbon atoms and D-F for oxygen atoms. Density is the probability of finding an interfacial atom at a given position in the (x,y) plane; high-density spots (from greenish to reddish patches) thus correspond to the most probable locations of the interfacial atoms. For both carbon and oxygen, the variations in the number of mPEG atoms exposed to the interface and their corresponding locations during the simulation indicate that mPEG chains are dynamic at the interface with water.

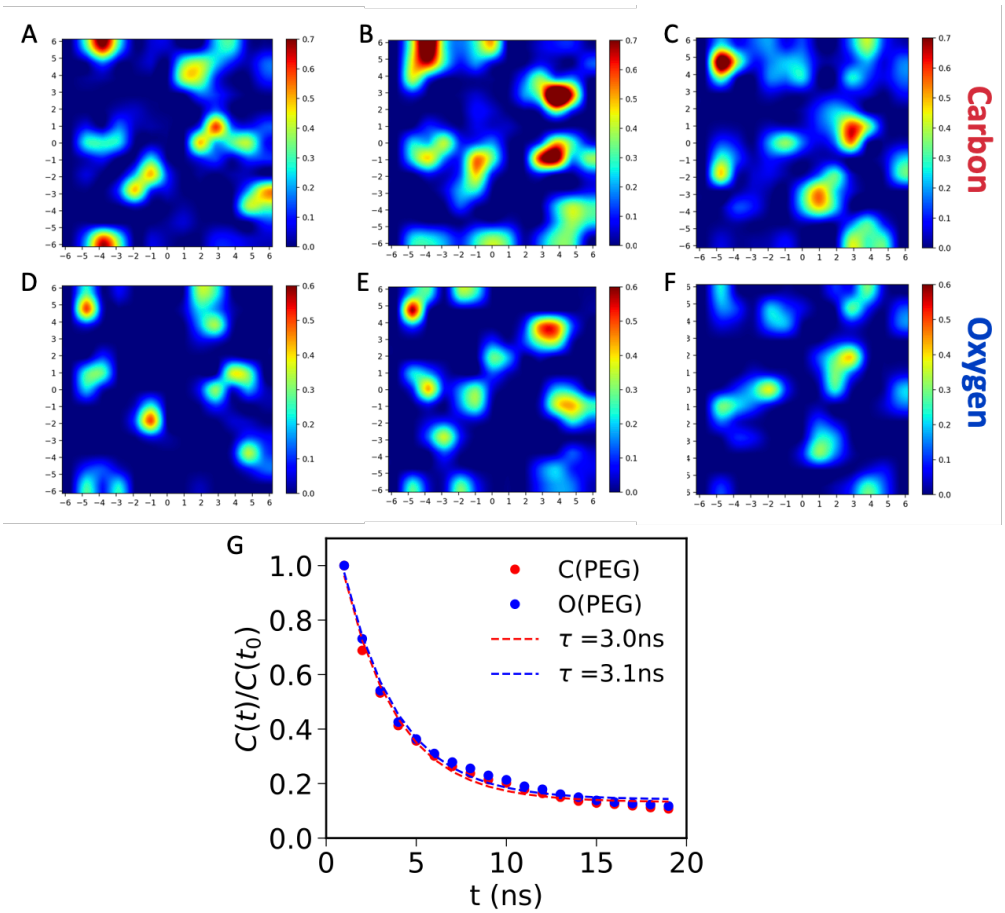

Figure 2: The ns dynamics of the methylated mPEG monolayer in contact with water. Representative density maps of mPEG carbon and oxygen atoms exposed to water (i.e., located within 3 Å to the instantaneous WC interface), averaged over different time periods along the DFT-MD simulation:[66] (A) from 0 to 50 ps, (B) from 200 to 250 ps, (C) from 350 to 400 ps. With time, the maps show the appearance and disappearance of red spots (density maxima). The red spots identify preferred locations for the exposed C and O atoms, which are dynamical, leading to time-fluctuating polar and apolar patches over the SAM surface. (G) The dynamics of these surface patches is characterized from classical MD (3x3 box, 80 ns simulation, see table 1), by means of the $C(t)/C(t_0)$ decay function, as defined in eqs. 2, 3. By exponential fitting of the decay functions for oxygen and carbon maps, characteristic times for surface pattern fluctuations on the order of 3 ns are derived.

The time scale of the dynamicity of mPEGs can be evaluated via the density maps of interfacial mPEG atoms, by taking inspiration from the decay function introduced in ref. 19 for metal/water interfaces. The idea of the approach is that time-resolved density plots reveal the location of interfacial mPEG atoms, which is heterogeneously distributed in the box when averaging over short time-scales. The more we increase the time interval over which

the maps are calculated, the more the map becomes homogeneous due to the dynamics of SAMs that expose their atoms all over the surface. The dynamics of mPEG chains can hence be quantified by the decay time of heterogeneity in the density maps while increasing the time lengths over which the maps are calculated. A long CMD trajectory of 80 ns is used to capture the ns time-scale.

In practice, following ref. 19, we denote the density maps of mPEG interfacial atoms as $M_{d_X}(t)$, where t is the time length over which the map is calculated, d_X signifies the density of interfacial mPEG atoms (X being either carbon or oxygen). The heterogeneity in mPEG surface distribution is quantified by calculating the spatial variance of these $M_{d_X}(t)$ maps:

$$C(t) = \langle \left[M_{d_X}\{x, y\}(t) - \bar{d}_X \right]^2 \rangle \tag{2}$$

where $M_{d_X}\{x, y\}(t)$ is the d_X density value at the {x, y} position in the map calculated over time t (i.e. by averaging between time t_0 and time t), $\bar{d}_X$ is the average density value over the whole box and over the total trajectory of 80 ns, and $\langle ... \rangle$ denotes averages over all grid points of the map.

The $C(t)/C(t_0)$ decay function of Fig. 2G is then constructed by normalizing $C(t)$ by the value at time t_0 and is plotted as a function of averaging time, t. $C(t)/C(t_0)$ is large for small t, since the surface pattern is heterogeneous, but exponentially decays to zero for large t values since the surface is dynamic, hence resulting in a homogeneous average map over sufficiently large time scales. To quantify the characteristic timescales, we fit $C(t)/C(t_0)$ by an exponential function:

$$C(t)/C(t_0) = A * exp(-\frac{t}{\tau}) + B \tag{3}$$

where τ is the relaxation time, i.e. the time scale of mPEG dynamics. τ values of 3.0 ns for carbon atoms and 3.1 ns for oxygen atoms are obtained, which indicates a ns dynamics of surface reorganization of mPEG in contact with liquid water.

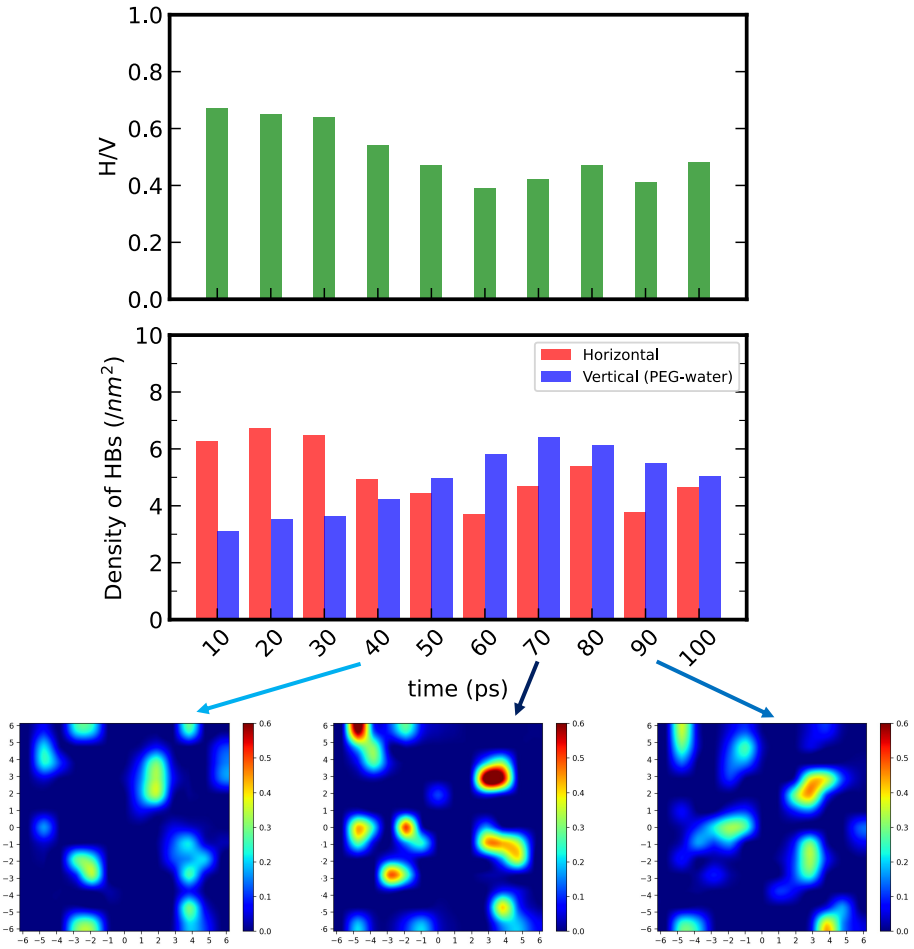

Figure 3: The mPEG chains dynamics induce time fluctuations in the interfacial H-bond network, hence in wetting. The surface wetting is evaluated as a function of time by the x_H descriptor. Upper panel: time-resolved x_H calculated over subsequent intervals of 10 ps, along a 100 ps portion of the DFT-MD simulation as an example. Lower panel: time-resolved "horizontal" and "vertical" H-bond-network components (reported as densities per nm^2), from which x_H is calculated with eq.1. Both panels show that the interfacial water H-bond network and wetting are time-dependent properties at the mSAM/water interface, which fluctuate in time in response to changes in the surface pattern (illustrated by three mPEG O-atoms density maps along the 100ps time window). For example, from 0 to 40 ps, fewer mPEG O-atoms are exposed to water (absence of red spots in the map) compared to the subsequent 40-80 ps period, and the water H-bond network reacts by assuming a horizontally dominated configuration, leading to a more hydrophobic interface (higher x_H).

Does the mPEG monolayer dynamicity influence wetting? To answer this question, we leverage on the time and spatially resolved H/V descriptor, x_H. We start from the time-

resolved x_H value obtained by averaging over each 10 ps during a 100 ps portion of the DFT-MD trajectory (Fig. 3). Even on the small simulation box and short time-scale of DFT-MD, we can already grasp the existence of a dynamicity in the wetting of the mPEG surface: x_H indeed fluctuates in time, and the fluctuations seem directly connected to changes in the SAM surface pattern, as shown by the accompanying mPEG-O-atoms density maps (constructed in the same way as the maps of Fig. 2). At the start of the monitored 100 ps period, only a few O-atoms are exposed by mPEG to water (absence of red spots in the 1^{st} map). The water H-bond network hence adapts by maximizing "horizontal" H-bonds between BIL-water molecules (red in the middle bar-plot of Fig. 3), resulting in the highest x_H value along these 100 ps ($\sim$0.6). With increasing time, around 70 ps, the PEG surface map becomes different, with clear red spots indicating an increase in the number of exposed O-atoms. The interfacial water network follows this change by increasing "vertical" H-bonds between BIL-water and PEG O-atoms (increase in the blue-bars height in the figure) and reducing "horizontal" H-bonds, leading to a reduction of x_H, i.e., to a more hydrophilic surface. Finally, at around 90 ps the surface pattern is again different, with less exposed O-atoms, and x_H starts to increase again accordingly. Surface wetting appears to be dynamic and to respond to the dynamics of the mPEG surface.

To better characterize local wetting and its dynamics, we spatially resolve in Fig.4 the changes of x_H on a large SAM surface (the 3×3 box from CMD). x_H maps are obtained by dividing the simulation box into grids of 6.6×6.6 Å^2, for a total of 36 grid squares. Over each square, the local density of "horizontal" and "vertical" H-bonds is calculated by only taking into account the BIL-water molecules whose xy coordinates are contained within the square (at each time step). The local x_H value is hence obtained with eq.1.

Fig. 4 compares time-averaged x_H maps over the whole trajectory of 1ns *vs* 80 ns. In the 1 ns x_H map, we observed dark-blueish patches ($x_H < 0.7$) corresponding to local hydrophilic patches, as well as reddish ($x_H > 0.8$) hydrophobic patches. The surface wetting is hence spatially heterogeneous over a ns timescale, with hydrophobic and hydrophilic patches

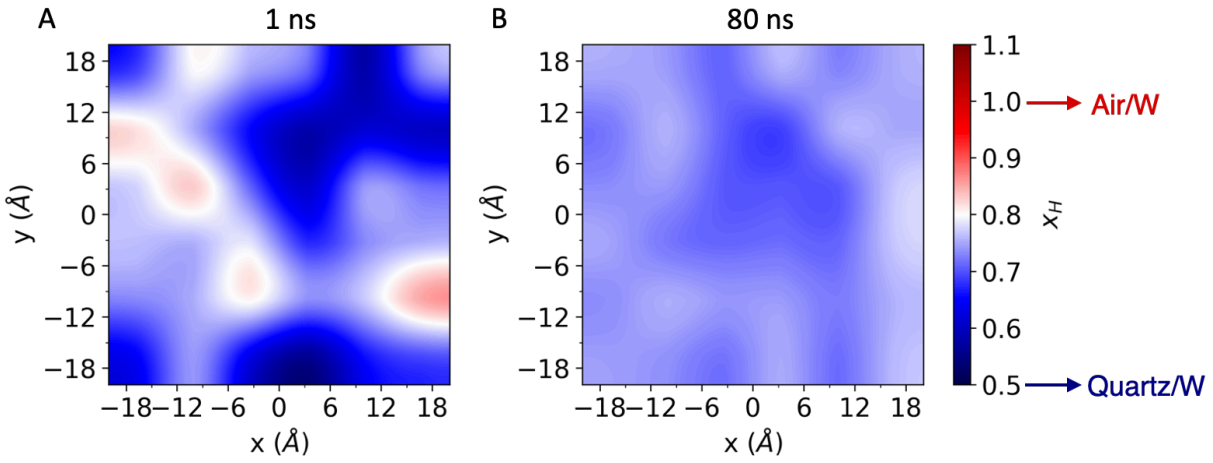

Figure 4: Spatially-resolving interfacial wetting: hydrophobic and hydrophilic patches dynamically appear on the mPEG surface. x_H maps of the PEG/water interface in the 3×3 box CMD simulations, calculated over (A) 1 ns trajectory and (B) 80 ns trajectory. In x_H maps, blueish patches ($x_H < 0.7$) correspond to local hydrophilic patches, and reddish patches ($x_H > 0.8$) are more hydrophobic. These patches are clearly visible when averaging over 1 ns, while they disappear over a longer time scale due to their dynamic nature. As shown by the color scale, the variations in local wetting are dramatic, from x_H values close to the air/water interface to x_H values typical of (super-) hydrophilic surfaces, such as α–Quartz. The local (in time and space) solvation properties are markedly different from the usually considered average properties.

of nano-meter size. Remarkably, the variations in local wetting across these patches are dramatic, from local x_H values close to 1, as at the prototypical hydrophobic air-water interface, to $x_H = 0.5$ as at the super-hydrophilic α–Quartz surface (as obtained from reference simulations[40,86]). However, the patches disappear when the x_H map is calculated over 80 ns, which highlights their dynamic character. Nanometric hydrophobic and hydrophilic patches hence dynamically appear on the mPEG surface, causing local (in time and space) solvation properties to be remarkably different from the usually considered average properties.

If such dynamical heterogeneity is really induced by the mPEG chains motions, then the time-scale over which hydrophobic/hydrophilic patches evolve must be commensurate to the 3ns mPEG surface dynamics (revealed by Fig. 2). To check this, we build a $M_{x_H}(t)$ matrix out of the x_H maps, as done before for the mPEG surface maps (eq.2), but now each $\mathbf{M}$ element corresponds to the local x_H value at the xy-grid element, averaged over the time interval, t.

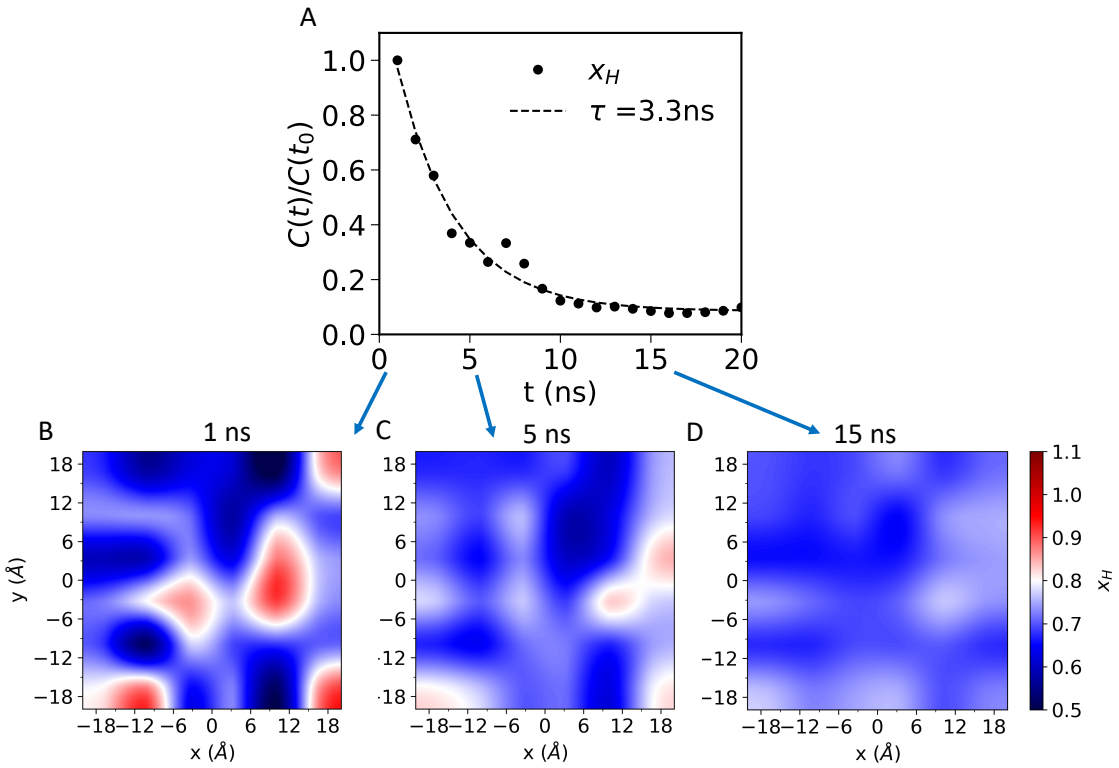

Figure 5: The dynamics of the hydrophilic/phobic patches follows the mPEG chains dynamics, resulting in spatial and time fluctuating wetting on a 3ns timescale. (A) Decay plot of the spatial variance ($C(t)/C(t_0)$) of the $M_{x_H}(t)$ maps, as obtained from the spatially and time-resolved x_H wetting descriptor using eq. 2. The fitted exponential function of the decay plot is plotted in dashed black, with a relaxation time of 3.3 ns, close to the values of 3.0 and 3.1 ns obtained from the mPEG chains $C(t)/C(t_0)$ decay plots of Fig. 2. Representative $M_{x_H}(t)$ maps averaged over (B) 1 ns, (C) 5 ns, and (D) 15 ns are also shown, illustrating the progressive disappearance of hydrophilic (blue) and hydrophobic (red) patches with increasing averaging time, t.

In analogy with our analysis of Fig. 2, we then construct the decay $C(t)/C(t_0)$ plot and fit it to an exponential function (eq. 3) to extract the characteristic time-scale of local surface wetting. The results are shown in Fig. 5, together with representative x_H maps illustrating the progressive disappearence of hydrophilic/phobic patches with increasing time-averaging.

Strikingly, the fitted exponential function yields a relaxation time of 3.3 ns, which matches well the 3.0/3.1 values obtained for mPEG dynamics. The local dynamics in surface wetting is hence dictated by the mPEG chain motions, which couple to the interfacial H-bond network, inducing rearrangements in "horizontal" and "vertical" H-bonds that modulate

wetting on the nano-meter size-scale and ns time-scale.

Conclusion

In summary, by combining DFT-MD and classical MD simulations of a methylated PEG monolayer/water interface, we observed a dynamical mPEG surface reorganization that strongly influences surface wetting. The methylation of PEG chains prevents the direct contact between the hydrophilic O atoms and water, hence triggering the fluctuations in the monolayer structure, which helps to expose the buried oxygen atoms to the interface. The mobility of the mPEG chains leads to the formation of nanometric patches with varying degrees of polarity (CH_3 rich or O rich), which are dynamic at nanosecond time scales. The water H-bond network adapts to these nanometric patches, resulting in local and dynamical wetting at the interface with the same nanosecond timescales, as revealed by our time- and space-resolved theoretical x_H descriptor.

Exciting implications of these findings can be imagined for interfacial science. For example, one could consider the interfacial patches as dynamical nano-reactors on the surface, where solvation properties and hence chemistry can markedly differ from the average surface. Their nanosecond dynamics is sufficiently slow to have crucial consequences for sub-nanosecond chemical and physical processes at the interface, such as ion adsorption and fast chemical reactions, e.g., proton and electron transfers, for which environmental and solvation effects play a crucial role. For these processes, it is the local and instantaneous surface wetting, rather than average properties measured experimentally, that matters.

Our results call for reevaluating our understanding of the solvation and chemistry at dynamically patterned surfaces, which must explicitly account for time fluctuations in local wetting. Furthermore, they may open interesting perspectives for manipulating interfacial chemistry since both the size- and length-scale of the hydrophobic/philic patches dynamics are determined by the surface composition, which can be altered, e.g., with mutations in the

case of biomolecules and surface functionalization in electrochemistry.

Acknowledgement

This work was performed under PRACE (Partnership for Advanced Computing in Europe), No. 2018194688. We acknowledge PRACE for awarding access to the Fenix infrastructures at GENCI-TGCC-France, which are partially funded by the European Union's Horizon 2020 research and innovation program through the ICEI project under the grant agreement No. 800858. We also acknowledge HPC resources from GENCI-France Grant 072484 (CINES/IDRIS/TGCC). S.P. acknowledges funding by the European Research Council (ERC, ELECTROPHOBIC, Grant Agreement No. 101077129). W.C. acknowledges support by the Alexander von Humboldt Foundation (AvH) for a research fellowship under the Henriette-Hertz-Scouting-Program. M.P. was supported by the Czech Science Foundation project 22-02972S.

References

(1) Rego, N. B.; Patel, A. J. Understanding hydrophobic effects: Insights from water density fluctuations. *Annual Review of Condensed Matter Physics* **2022**, *13*, 303–324.

(2) Chandler, D. Interfaces and the driving force of hydrophobic assembly. *Nature* **2005**, *437*, 640–647.

(3) Bañuelos, J. L.; Borguet, E.; Brown Jr, G. E.; Cygan, R. T.; DeYoreo, J. J.; Dove, P. M.; Gaigeot, M.-P.; Geiger, F. M.; Gibbs, J. M.; Grassian, V. H., et al. Oxide–and silicate–water interfaces and their roles in technology and the environment. *Chem. Rev.* **2023**, *123*, 6413–6544.

(4) Gonella, G.; Backus, E. H.; Nagata, Y.; Bonthuis, D. J.; Loche, P.; Schlaich, A.;

Netz, R. R.; Kühnle, A.; McCrum, I. T.; Koper, M. T., et al. Water at charged interfaces. *Nature Reviews Chemistry* **2021**, *5*, 466–485.

(5) Verdaguer, A.; Sacha, G.; Bluhm, H.; Salmeron, M. Molecular structure of water at interfaces: Wetting at the nanometer scale. *Chemical reviews* **2006**, *106*, 1478–1510.

(6) Sinha Mahapatra, P.; Ganguly, R.; Ghosh, A.; Chatterjee, S.; Lowrey, S.; Sommers, A. D.; Megaridis, C. M. Patterning wettability for open-surface fluidic manipulation: fundamentals and applications. *Chemical reviews* **2022**, *122*, 16752–16801.

(7) Ball, P. Water as an active constituent in cell biology. *Chemical reviews* **2008**, *108*, 74–108.

(8) 't Mannetje, D.; Ghosh, S.; Lagraauw, R.; Otten, S.; Pit, A.; Berendsen, C.; Zeegers, J.; van den Ende, D.; Mugele, F. Trapping of drops by wetting defects. *Nature communications* **2014**, *5*, 3559.

(9) Petersen, P. B.; Saykally, R. J. On the nature of ions at the liquid water surface. *Annu. Rev. Phys. Chem.* **2006**, *57*, 333–364.

(10) Devlin, S. W.; Benjamin, I.; Saykally, R. J. On the mechanisms of ion adsorption to aqueous interfaces: air-water vs. oil-water. *Proceedings of the National Academy of Sciences* **2022**, *119*, e2210857119.

(11) Limaye, A.; Suvlu, D.; Willard, A. P. Water molecules mute the dependence of the double-layer potential profile on ionic strength. *Faraday Discussions* **2024**, *249*, 267–288.

(12) Giovambattista, N.; Debenedetti, P. G.; Rossky, P. J. Hydration behavior under confinement by nanoscale surfaces with patterned hydrophobicity and hydrophilicity. *J. Phys. Chem. C* **2007**, *111*, 1323–1332.

(13) Lee, C.-Y.; McCammon, J. A.; Rossky, P. The structure of liquid water at an extended hydrophobic surface. *J. Chem. Phys.* **1984**, *80*, 4448–4455.

(14) Mamatkulov, S. I.; Khabibullaev, P. K.; Netz, R. R. Water at hydrophobic substrates: curvature, pressure, and temperature effects. *Langmuir* **2004**, *20*, 4756–4763.

(15) Jamadagni, S. N.; Godawat, R.; Garde, S. Hydrophobicity of proteins and interfaces: Insights from density fluctuations. *Annu. Rev. Chem. Biomol.* **2011**, *2*, 147–171.

(16) Xi, E.; Venkateshwaran, V.; Li, L.; Rego, N.; Patel, A. J.; Garde, S. Hydrophobicity of proteins and nanostructured solutes is governed by topographical and chemical context. *Proc. Natl. Acad. Sci.* **2017**, *114*, 13345–13350.

(17) Rego, N. B.; Ferguson, A. L.; Patel, A. J. Learning the relationship between nanoscale chemical patterning and hydrophobicity. *Proc. Natl. Acad. Sci.* **2022**, *119*, e2200018119.

(18) Rego, N. B.; Xi, E.; Patel, A. J. Identifying hydrophobic protein patches to inform protein interaction interfaces. *Proc. Natl. Acad. Sci.* **2021**, *118*.

(19) Limmer, D. T.; Willard, A. P.; Madden, P.; Chandler, D. Hydration of metal surfaces can be dynamically heterogeneous and hydrophobic. *Proc. Natl. Acad. Sci.* **2013**, *110*, 4200–4205.

(20) Cyran, J. D.; Donovan, M. A.; Vollmer, D.; Brigiano, F. S.; Pezzotti, S.; Galimberti, D. R.; Gaigeot, M.-P.; Bonn, M.; Backus, E. H. Molecular hydrophobicity at a macroscopically hydrophilic surface. *Proc. Natl. Acad. Sci.* **2019**, *116*, 1520–1525.

(21) Tuladhar, A.; Dewan, S.; Pezzotti, S.; Brigiano, F. S.; Creazzo, F.; Gaigeot, M.-P.; Borguet, E. Ions tune interfacial water structure and modulate hydrophobic interactions at silica surfaces. *J. Am. Chem. Soc.* **2020**, *142*, 6991–7000.

(22) Wang, R.; DelloStritto, M.; Klein, M. L.; Borguet, E.; Carnevale, V. Topological properties of interfacial hydrogen bond networks. *Physical Review B* **2024**, *110*, 014105.

(23) Kronberg, B. The hydrophobic effect. *Current Opinion in Colloid & Interface Science* **2016**, *22*, 14–22.

(24) Patel, A. J.; Varilly, P.; Chandler, D. Fluctuations of water near extended hydrophobic and hydrophilic surfaces. *J. Phys. Chem. B* **2010**, *114*, 1632–1637.

(25) Monroe, J.; Barry, M.; DeStefano, A.; Gokturk, P. A.; Jiao, S.; Robinson-Brown, D.; Webber, T.; Crumlin, E. J.; Han, S.; Shell, M. S. Water Structure and Properties at Hydrophilic and Hydrophobic Surfaces. *Annu. Rev. Chem. Biomol.* **2020**, *11*, 523–557.

(26) Jiao, S.; Shell, M. S. Inverse design of pore wall chemistry and topology through active learning of surface group interactions. *J. Chem. Phys.* **2024**, *160*.

(27) Mukherjee, S.; Schäfer, L. V. Spatially Resolved Hydration Thermodynamics in Biomolecular Systems. *J. Phys. Chem. B* **2022**, *126*, 3619–3631.

(28) Adams, E. M.; Pezzotti, S.; Ahlers, J.; Rüttermann, M.; Levin, M.; Goldenzweig, A.; Peleg, Y.; Fleishman, S. J.; Sagi, I.; Havenith, M. Local Mutations Can Serve as a Game Changer for Global Protein Solvent Interaction. *JACS Au* **2021**, *1*, 1076–1085.

(29) Pezzotti, S.; König, B.; Ramos, S.; Schwaab, G.; Havenith, M. Liquid–Liquid Phase Separation? Ask the Water! *J. Phys. Chem. Lett.* **2023**, *14*, 1556–1563.

(30) Huang, D. M.; Chandler, D. Temperature and length scale dependence of hydrophobic effects and their possible implications for protein folding. *Proc. Natl. Acad. Sci.* **2000**, *97*, 8324–8327.

(31) Shin, S.; Willard, A. P. Characterizing hydration properties based on the orientational structure of interfacial water molecules. *J. Chem. Theory Comput.* **2018**, *14*, 461–465.

(32) Tocci, G.; Joly, L.; Michaelides, A. Friction of water on graphene and hexagonal boron nitride from ab initio methods: very different slippage despite very similar interface structures. *Nano letters* **2014**, *14*, 6872–6877.

(33) Monroe, J. I.; Shell, M. S. Computational discovery of chemically patterned surfaces that effect unique hydration water dynamics. *Proc. Natl. Acad. Sci.* **2018**, *115*, 8093–8098.

(34) Dill, K. A.; Ozkan, S. B.; Shell, M. S.; Weikl, T. R. The protein folding problem. *Annu. Rev. Biophys.* **2008**, *37*, 289–316.

(35) M., B. J.; Q., Y.; F., S. B.; W., C.; S., P. On the Chemistry at Oxide/Water Interfaces: the Role of Interfacial Water. *ChemRxiv* **2024**, 10.26434/chemrxiv–2024–snt1m.

(36) Ugliengo, P.; Sodupe, M.; Musso, F.; Bush, I.; Orlando, R.; Dovesi, R. Realistic models of hydroxylated amorphous silica surfaces and MCM-41 mesoporous material simulated by large-scale periodic B3LYP calculations. *Adv. Mater.* **2008**, *20*, 4579–4583.

(37) Rimola, A.; Costa, D.; Sodupe, M.; Lambert, J.-F.; Ugliengo, P. Silica Surface Features and Their Role in the Adsorption of Biomolecules: Computational Modeling and Experiments. **2013**,

(38) Liu, W.-T.; Shen, Y. Surface vibrational modes of α-quartz (0001) probed by sum-frequency spectroscopy. *Phys. Rev. Lett.* **2008**, *101*, 016101.

(39) Hassanali, A. A.; Singer, S. J. Model for the water- amorphous silica interface: the undissociated surface. *The Journal of Physical Chemistry B* **2007**, *111*, 11181–11193.

(40) Pezzotti, S.; Serva, A.; Sebastiani, F.; Brigiano, F. S.; Galimberti, D. R.; Potier, L.; Alfarano, S.; Schwaab, G.; Havenith, M.; Gaigeot, M.-P. Molecular fingerprints of hydrophobicity at aqueous interfaces from theory and vibrational spectroscopies. *J. Phys. Chem. Lett.* **2021**, *12*, 3827–3836.

(41) Rimola, A.; Costa, D.; Sodupe, M.; Lambert, J.-F.; Ugliengo, P. Silica surface features and their role in the adsorption of biomolecules: computational modeling and experiments. **2013**, *113*, 4216–4313.

(42) Rotenberg, B.; Patel, A. J.; Chandler, D. Molecular explanation for why talc surfaces can be both hydrophilic and hydrophobic. *J. Am. Chem. Soc.* **2011**, *133*, 20521–20527.

(43) Serva, A.; Salanne, M.; Havenith, M.; Pezzotti, S. Size dependence of hydrophobic hydration at electrified gold/water interfaces. *Proc. Natl. Acad. Sci.* **2021**, *118*.

(44) Alfarano, S. R. et al. Stripping away ion hydration shells in electrical double-layer formation: Water networks matter. *Proc. Natl. Acad. Sci.* **2021**, *118*.

(45) Eggert, T.; Hörmann, N. G.; Reuter, K. Cavity formation at metal–water interfaces. *J. Chem. Phys.* **2023**, *159*.

(46) Qu, M.; Huang, G.; Liu, X.; Nie, X.; Qi, C.; Wang, H.; Hu, J.; Fang, H.; Gao, Y.; Liu, W.-T., et al. Room temperature bilayer water structures on a rutile TiO 2 (110) surface: hydrophobic or hydrophilic? *Chemical Science* **2022**, *13*, 10546–10554.

(47) Serva, A.; Pezzotti, S. S.O.S: Shape, orientation, and size tune solvation in electrocatalysis. *J. Chem. Phys.* **2024**, *160*, 094707.

(48) Serva, A.; Havenith, M.; Pezzotti, S. The role of hydrophobic hydration in the free energy of chemical reactions at the gold/water interface: Size and position effects. *J. Chem. Phys.* **2021**, *155*, 204706.

(49) Murke, S.; Chen, W.; Pezzotti, S.; Havenith, M. Tuning Acid–Base Chemistry at an Electrified Gold/Water Interface. *J. Am. Chem. Soc.* **2024**,

(50) Dubouis, N.; Serva, A.; Berthin, R.; Jeanmairet, G.; Porcheron, B.; Salager, E.; Salanne, M.; Grimaud, A. Tuning water reduction through controlled nanoconfinement within an organic liquid matrix. *Nat. Catal.* **2020**, *3*, 656–663.

(51) Li, P.; Jiang, Y.; Hu, Y.; Men, Y.; Liu, Y.; Cai, W.; Chen, S. Hydrogen bond network connectivity in the electric double layer dominates the kinetic pH effect in hydrogen electrocatalysis on Pt. *Nat. Catal.* **2022**, *5*, 900–911.

(52) Liang, H.-Q.; Zhao, S.; Hu, X.-M.; Ceccato, M.; Skrydstrup, T.; Daasbjerg, K. Hydrophobic copper interfaces boost electroreduction of carbon dioxide to ethylene in water. *ACS Catal.* **2021**, *11*, 958–966.

(53) Willard, A. P.; Reed, S. K.; Madden, P. A.; Chandler, D. Water at an electrochemical interface - a simulation study. *Faraday Discuss.* **2009**, *141*, 423–441.

(54) Willard, A. P.; Limmer, D. T.; Madden, P. A.; Chandler, D. Characterizing heterogeneous dynamics at hydrated electrode surfaces. *The Journal of chemical physics* **2013**, *138*.

(55) Zhang, L.; Yang, Y.; Kao, Y.-T.; Wang, L.; Zhong, D. Protein Hydration Dynamics and Molecular Mechanism of Coupled Water?Protein Fluctuations. *J. Am. Chem. Soc.* **2009**, *131*, 10677–10691.

(56) Markelz, A. G.; Mittleman, D. M. Perspective on Terahertz Applications in Bioscience and Biotechnology. *ACS Photonics* **2022**, *9*, 1117–1126.

(57) Markelz, A.; Roitberg, A.; Heilweil, E. J. Pulsed terahertz spectroscopy of DNA, bovine serum albumin and collagen between 0.1 and 2.0 THz. *Chem. Phys. Lett.* **2000**, *320*, 42–48.

(58) Austin, R. H.; Beeson, K.; Eisenstein, L.; Frauenfelder, H.; Gunsalus, I. Dynamics of ligand binding to myoglobin. *Biochemistry* **1975**, *14*, 5355–5373.

(59) Riedel, C.; Gabizon, R.; Wilson, C. A.; Hamadani, K.; Tsekouras, K.; Marqusee, S.; Pressé, S.; Bustamante, C. The heat released during catalytic turnover enhances the diffusion of an enzyme. *Nature* **2015**, *517*, 227–230.

(60) Pireddu, G.; Rotenberg, B. Frequency-dependent impedance of nanocapacitors from electrode charge fluctuations as a probe of electrolyte dynamics. *Physical Review Letters* **2023**, *130*, 098001.

(61) Hoberg, C.; Talbot, J. J.; Shee, J.; Ockelmann, T.; Mahanta, D. D.; Novelli, F.; Head-Gordon, M.; Havenith, M. Caught in the act: real-time observation of the solvent response that promotes excited-state proton transfer in pyranine. *Chemical Science* **2023**, *14*, 4048–4058.

(62) Wolke, C. T.; Fournier, J. A.; Dzugan, L. C.; Fagiani, M. R.; Odbadrakh, T. T.; Knorke, H.; Jordan, K. D.; McCoy, A. B.; Asmis, K. R.; Johnson, M. A. Spectroscopic snapshots of the proton-transfer mechanism in water. *Science* **2016**, *354*, 1131–1135.

(63) Eftekhari-Bafrooei, A.; Borguet, E. Effect of electric fields on the ultrafast vibrational relaxation of water at a charged solid–liquid interface as probed by vibrational sum frequency generation. *The Journal of Physical Chemistry Letters* **2011**, *2*, 1353–1358.

(64) Nihonyanagi, S.; Yamaguchi, S.; Tahara, T. Ultrafast dynamics at water interfaces studied by vibrational sum frequency generation spectroscopy. *Chemical Reviews* **2017**, *117*, 10665–10693.

(65) Sanders, S. E.; Petersen, P. B. Heterodyne-detected sum frequency generation of water at surfaces with varying hydrophobicity. *J. Chem. Phys.* **2019**, *150*, 204708.

(66) Chen, W.; Sanders, S. E.; Ozdamar, B.; Louaas, D.; Brigiano, F. S.; Pezzotti, S.; Petersen, P. B.; Gaigeot, M.-P. On the trail of molecular hydrophilicity and hydrophobicity at aqueous interfaces. *J. Phys. Chem. Lett.* **2023**, *14*, 1301–1309.

(67) Lee, C.; Yang, W.; Parr, R. G. Development of the Colle-Salvetti correlation-energy formula into a functional of the electron density. *Phys. Rev. B* **1988**, *37*, 785.

(68) Becke, A. D. Density-functional exchange-energy approximation with correct asymptotic behavior. *Phys. Rev. A* **1988**, *38*, 3098.

(69) Grimme, S. Accurate description of van der Waals complexes by density functional theory including empirical corrections. *J. Comput. Chem.* **2004**, *25*, 1463–1473.

(70) Grimme, S. Semiempirical GGA-type density functional constructed with a long-range dispersion correction. *J. Comput. Chem.* **2006**, *27*, 1787–1799.

(71) Van Der Spoel, D.; Lindahl, E.; Hess, B.; Groenhof, G.; Mark, A. E.; Berendsen, H. J. C. GROMACS: Fast, Flexible, and Free. *J. Comput. Chem.* **2005**, *26*, 1701–1718.

(72) Roscioni, O. M.; Muccioli, L.; Mityashin, A.; Cornil, J.; Zannoni, C. Structural characterization of alkylsilane and fluoroalkylsilane self-assembled monolayers on SiO2 by molecular dynamics simulations. *J. Phys. Chem. C* **2016**, *120*, 14652–14662.

(73) Cygan, R. T.; Liang, J.-J.; Kalinichev, A. G. Molecular models of hydroxide, oxyhydroxide, and clay phases and the development of a general force field. *J. Phys. Chem. B* **2004**, *108*, 1255–1266.

(74) Mityashin, A.; Roscioni, O. M.; Muccioli, L.; Zannoni, C.; Geskin, V.; Cornil, J.; Janssen, D.; Steudel, S.; Genoe, J.; Heremans, P. Multiscale modeling of the electrostatic impact of self-assembled monolayers used as gate dielectric treatment in organic thin-film transistors. *ACS Appl. Mater. Interfaces* **2014**, *6*, 15372–15378.

(75) Wang, J.; Wolf, R. M.; Caldwell, J. W.; Kollman, P. A.; Case, D. A. Development and testing of a general amber force field. *J. Comput. Chem.* **2004**, *25*, 1157–1174.

(76) Bayly, C. I.; Cieplak, P.; Cornell, W.; Kollman, P. A. A well-behaved electrostatic potential based method using charge restraints for deriving atomic charges: the RESP model. *J. Phys. Chem.* **1993**, *97*, 10269–10280.

(77) Marti, J.; Padró, J.; Guardia, E. Molecular dynamics calculation of the infrared spectra in liquid H2O-D2O mixtures. *J. Mol. Liq.* **1994**, *62*, 17–31.

(78) Kroutil, O.; Pezzotti, S.; Gaigeot, M.-P.; Předota, M. Phase-Sensitive Vibrational SFG Spectra from Simple Classical Force Field Molecular Dynamics Simulations. *jpcc* **2020**, *124*, 15253–15263.

(79) Nosé, S. A unified formulation of the constant temperature molecular dynamics methods. *J. Chem. Phys.* **1984**, *81*, 511–519.

(80) Hoover, W. G. Canonical dynamics: Equilibrium phase-space distributions. *Phys. Rev. A* **1985**, *31*, 1695–1697.

(81) Khatib, R.; Backus, E. H.; Bonn, M.; Perez-Haro, M.-J.; Gaigeot, M.-P.; Sulpizi, M. Water orientation and hydrogen-bond structure at the fluorite/water interface. *Sci. Rep.* **2016**, *6*, 1–10.

(82) Pezzotti, S.; Galimberti, D. R.; Shen, Y. R.; Gaigeot, M.-P. Structural definition of the BIL and DL: A new universal methodology to rationalize non-linear $\chi^{(2)}(\omega)$ SFG signals at charged interfaces, including $\chi^{(3)}(\omega)$ contributions. *Phys. Chem. Chem. Phys.* **2018**, *20*, 5190–5199.

(83) Chen, W.; Louaas, D.; Brigiano, F. S.; Pezzotti, S.; Gaigeot, M.-P. A Simplified Method for Theoretical Sum Frequency Generation Spectroscopy Calculation and Interpretation: the "pop model". *ChemRxiv* **2023**,

(84) Wen, Y.-C.; Zha, S.; Liu, X.; Yang, S.; Guo, P.; Shi, G.; Fang, H.; Shen, Y. R.; Tian, C. Unveiling microscopic structures of charged water interfaces by surface-specific vibrational spectroscopy. *Phys. Rev. Lett.* **2016**, *116*, 016101.

(85) Dalstein, L.; Chiang, K.-Y.; Wen, Y.-C. Direct quantification of water surface charge by phase-sensitive second harmonic spectroscopy. *The Journal of Physical Chemistry Letters* **2019**, *10*, 5200–5205.

(86) Pezzotti, S.; Galimberti, D. R.; Gaigeot, M.-P. Deconvolution of BIL-SFG and DL-SFG spectroscopic signals reveals order/disorder of water at the elusive aqueous silica interface. *Phys. Chem. Chem. Phys.* **2019**, *21*, 22188–22202.

(87) Pezzotti, S.; Galimberti, D. R.; Shen, Y. R.; Gaigeot, M.-P. What the diffuse layer (DL) reveals in non-linear SFG spectroscopy. *Minerals* **2018**, *8*, 305.

(88) Willard, A. P.; Chandler, D. Instantaneous liquid interfaces. *J. Phys. Chem. B* **2010**, *114*, 1954–1958.

(89) Pezzotti, S.; Galimberti, D. R.; Gaigeot, M.-P. 2D H-bond network as the topmost skin to the air–water interface. *J. Phys. Chem. Lett.* **2017**, *8*, 3133–3141.

(90) Pezzotti, S.; Sebastiani, F.; van Dam, E. P.; Ramos, S.; Conti Nibali, V.; Schwaab, G.; Havenith, M. Spectroscopic fingerprints of cavity formation and solute insertion as a measure of hydration entropic loss and enthalpic gain. *Angew. Chem. Int. Ed.* **2022**, *134*, e202203893.

(91) Wang, R.; Zou, Y.; Remsing, R. C.; Ross, N. O.; Klein, M. L.; Carnevale, V.; Borguet, E. Superhydrophilicity of α-alumina surfaces results from tight binding of interfacial waters to specific aluminols. *J. Colloid Interface Sci.* **2022**, *628*, 943–954.

(92) Godawat, R.; Jamadagni, S. N.; Garde, S. Characterizing hydrophobicity of interfaces by using cavity formation, solute binding, and water correlations. *Proc. Natl. Acad. Sci.* **2009**, *106*, 15119–15124.

(93) Acharya, H.; Vembanur, S.; Jamadagni, S. N.; Garde, S. Mapping hydrophobicity at the nanoscale: Applications to heterogeneous surfaces and proteins. *Faraday Discuss.* **2010**, *146*, 353–365.

(94) Lum, K.; Chandler, D.; Weeks, J. D. Hydrophobicity at Small and Large Length Scales. *J. Phys. Chem. B* **1999**, *103*, 4570–4577.

(95) White, J. A.; Schwegler, E.; Galli, G.; Gygi, F. The solvation of Na^+ in water: First-principles simulations. *J. Chem. Phys.* **2000**, *113*, 4668–4673.

(96) Luzar, A.; Chandler, D. Structure and hydrogen bond dynamics of water–dimethyl sulfoxide mixtures by computer simulations. *The Journal of chemical physics* **1993**, *98*, 8160–8173.